

## Complex Behavior of Caffeine Crystallites on Muscovite Mica Surfaces

Christian Röthel,<sup>\*,†,§</sup> Michal Radziown,<sup>‡</sup> Roland Resel,<sup>§</sup> Andreas Zimmer,<sup>†</sup> Clemens Simbrunner,<sup>‡,¶</sup> and Oliver Werzer<sup>\*,†</sup>

<sup>†</sup>Institute of Pharmaceutical Sciences, Department of Pharmaceutical Technology, Karl-Franzens Universität Graz, Universitätsplatz 1, 8010 Graz, Austria

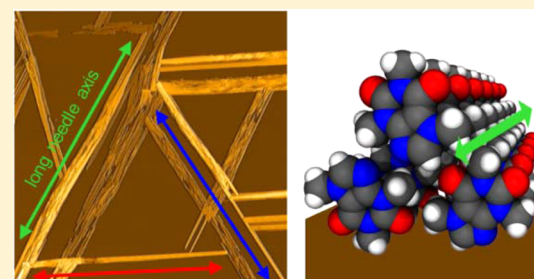
<sup>§</sup>Institute of Solid State Physics, Graz University of Technology, Petersgasse 16, 8010 Graz, Austria

<sup>‡</sup>Institute of Semiconductor and Solid State Physics, Johannes Kepler Universität Linz, Altenbergerstraße 69, 4040 Linz, Austria

<sup>¶</sup>Institute of Solid State Physics, University of Bremen, Otto-Hahn-Allee 1, 28359 Bremen, Germany

### Supporting Information

**ABSTRACT:** Defined fabrication of organic thin films is highly desired in technological, as well as pharmaceutical, applications since morphology and crystal structure are directly linked to physical, electrical, and optical properties. Within this work, the directed growth of caffeine deposited by hot wall epitaxy (HWE) on muscovite mica is studied. Optical and atomic force microscopy measurements reveal the presence of caffeine needles exhibiting a preferable alignment in the azimuthal directions with respect to the orientation of the defined mica surface. Specular X-ray diffraction and X-ray diffraction pole figure measurements give evidence that the  $\beta$ -polymorphic form of caffeine forms on the mica surface. All results consent that caffeine molecules have an edge-on conformation i.e. minimizing their interaction area with the surface. Furthermore, the azimuthal alignment of the long caffeine needle axis takes place along the  $[1\bar{1}0]$ ,  $[100]$ , and  $[110]$  real space directions of mica; needles are observed every  $60^\circ$  azimuthally. While mica has a complex surface structure with mirror planes and lowered oxygen rows, the slightly disturbed 3-fold symmetry dictates the crystal alignment. This is different to previous findings for solution cast caffeine growth on mica. For HWE the needles align solely along the mica main directions whereby solution cast needles show an additional needle splitting due to a different alignment of caffeine with respect to the surface.



### INTRODUCTION

In recent years defined preparation of thin films has become highly desired since many technological applications or fundamental studies<sup>1–4</sup> depend on the reliable and controlled fabrication of organic, inorganic, or metallic thin films. The variation of process parameters such as temperature, pressure, deposition rate, and environment (e.g., solvent), allows engineering thin films with particular properties and morphologies.<sup>5,6</sup> This in turn tunes for instance the optical,<sup>7,8</sup> and electrical properties.<sup>9,10</sup> Especially the control of the solid state properties, such as polymorphism<sup>11,12</sup> or morphology, are of outmost interest for pharmaceutical drug formulation since this is one of the decisive factors for drug release and resorption in living organisms (bioavailability).<sup>13</sup>

A well-established method for thin film preparation with high scientific but also industrial relevance<sup>14</sup> is physical vapor deposition (PVD). Even though PVD is especially appealing since the thin film preparation is carried out under specific environmental conditions, such as ultrahigh vacuum or in inert gas atmosphere, it is hardly recognized in pharmaceutical science. However, PVD as a solventless process allows for limiting the interaction during crystal growth to solely

molecule–molecule and molecule–substrate interactions which helps to identify the underlying growth mechanisms. More importantly, contingent interactions for example with solvents or ambient atmosphere (especially with surface water), are mostly avoided during film formation easing the understanding of heterogeneous crystal growth.

Despite the process parameters, the choice of substrate has a strong influence on film formation and crystal growth. During crystallization, interactions of the organic molecules with the substrate surface because of van der Waals forces, H-bonding, or electrostatics play a decisive role.<sup>15</sup> It was demonstrated previously, that crystallization in proximity of solid surfaces is able to increase the crystal yield, aid the growth of certain polymorphs,<sup>16</sup> or induce directional growth.<sup>17</sup> Moreover, surfaces are able to stabilize certain fragile polymorphs<sup>18</sup> for a prolonged timespan or induce/mediate new polymorphs which are not accessible by conventional bulk methods.<sup>19</sup> Typically substrates are classified based on their surface properties.

**Received:** June 15, 2015

**Revised:** July 30, 2015

**Published:** July 31, 2015

Isotropic surfaces contain randomly arranged atoms at the solid–air interface without long-range order, such as conventional glass surfaces, indium–tin oxide (ITO) layers,<sup>20</sup> polymer surfaces,<sup>21</sup> or self-assembled monolayers.<sup>22</sup> Generally, such surfaces are only capable of selecting a preferred contact plane of a molecular crystal during a PVD process resulting in azimuthally randomly distributed crystals on the surface.<sup>23</sup> In contrast, highly anisotropic surfaces are present, for instance, in rubbed polymer surface,<sup>21</sup> or outer/cleaved surfaces<sup>24</sup> of single crystal minerals, salts, inorganics, metals,<sup>25</sup> or others. Some of the most prominent examples for such surfaces are mica,<sup>26</sup> NaCl, silicon,<sup>27</sup> or gold. The particular periodic arrangement at the surface depends on the chemical composition and their ability to rearrange. For instance different cutting direction of the crystal results in altered surface properties which in turn might facilitate the heterogeneous crystal growth.<sup>28</sup>

Many PVD studies on thin film growth focus on synthetic, highly symmetric, conjugated organic molecules because of their importance for application in organic electronics.<sup>29–32</sup> However, most drug molecules feature asymmetric chemical structures with quasi ambipolar character. This accounts on the one hand for aqueous solubility, on the other hand, dependent on its partition coefficient ( $\log P$ ), the ambipolarity allows for cell membrane penetration.<sup>33</sup> In order to study the growth of such asymmetric molecules on a solid surface, caffeine is an ideal model candidate as it is widely used in pharmaceuticals as pure active pharmaceutical ingredient (API), as excipient in pain killers and as a cocrystallization agent for various molecules.<sup>34–36</sup> Caffeine is typically purified via sublimation and recrystallization. However, for such a procedure low process control is required, thus preknowledge of caffeine deposition behavior within a controlled PVD process is rather limited.<sup>37</sup> There are studies of caffeine on various surfaces deposited from solution, showing the growth of either needle-like morphology or plate-like hexagons with the surface having a decisive impact on the crystal alignment.<sup>38,39</sup> Previous studies on solution cast samples show that caffeine deposited onto mica surfaces results in an alignment of caffeine with respect to the underlying mica surface.<sup>40</sup>

There are many PVD processes described in literature ranging from simple vacuum apparatus to very sophisticated ultrahigh vacuum chamber assemblies.<sup>41</sup> For organic thin films, a hot wall epitaxy setup (HWE)<sup>42</sup> is well suited since it works close to thermodynamic equilibrium and facilitates the growth of van der Waals bonded systems.<sup>43</sup> In the case of caffeine a reduction of the pressure is not required as heating of caffeine to 120 °C at ambient pressure results in excessive sublimation. Furthermore, having an inert gas along the heated deposition cone (hot wall) at ambient pressure is sufficient to achieve caffeine films of very high quality. Mica is used in this study as it is atomically flat and is furthermore capable of aligning molecules along specific directions as reported for various organic systems.<sup>17,40</sup> The resulting thin films will be investigated by microscopy and X-ray based techniques allowing the caffeine crystallization at the surface to be understood. Similarities or differences to caffeine crystal growth on mica by solution casting are elucidated.

## ■ EXPERIMENTAL SECTION

**Materials.** Samples were prepared on muscovite mica (001) substrates (grade V-4) purchased from SPI Supplies (West Chester, USA). All substrate surfaces were cleaved freshly and immediately transferred into the HWE chamber. Caffeine (pharmaceutical grade)

was purchased from Herba Chemosan-AG (Vienna, Austria) and used without further treatment.

**Sample Preparation.** Prior deposition the mica substrates were preheated for 30 min at the desired substrate temperature of 65 °C to ensure thermal stability. After preheating, a shutter was opened and the mica surfaces were exposed to the molecular flux for 5, 10, 15, and 20 min. Optimal temperature setting of 125 °C for the source and 130 °C for the wall have been obtained and kept constant for all depositions in this study.

**X-ray Diffraction Experiments.** Specular X-ray diffraction (SXRD) measurements were performed on a PANalytical EMPYREAN reflectometer fitted with a Cu sealed tube ( $\lambda = 1.54 \text{ \AA}$ ), a 1/32° primary slit, a 10 mm beam mask and a multilayer mirror on the primary side. On the secondary side a slit system containing a 0.1 mm receiving slit and 0.02 rad Soller slits defined the diffracted beam. The intensities as a function of the scattering angle were recorded using a 3D PANalytical PIXcel detector.

X-ray pole figures (XRPF) were performed on a Philips X'pert diffractometer using a chromium sealed tube and secondary graphite monochromator ( $\lambda = 2.29 \text{ \AA}$ ). Pole figures were recorded for a fixed scattering vector  $|q|$  in Schutz reflective geometry.<sup>44</sup> Shortly, an X-ray diffraction pole figure contains information about the spatial distribution of specific net planes with respect to the substrate surface. During the measurement the sample is rotated around the Eulerian angles  $\psi$  (inclination of the surface normal) and  $\varphi$  (rotation around the surface normal). The intensity data is presented in polar contour plots with  $\psi$  being the polar radius and  $\varphi$  the polar angle. Spots with enhanced intensity (poles) correspond to Bragg reflections which are caused by net planes which fulfill the Laue condition, meaning the corresponding net planes are normal to pole direction. Experimental data was visualized and evaluated using the software STEREOPOLE.<sup>45</sup>

**Morphological Investigation.** Optical microscope images were taken with an Axiovert 40 microscope (Zeiss, Germany) equipped with a high resolution digital camera. Atomic force microscopy (AFM) height measurements were performed using a FlexAFM and Easyscan 2 controller (Nanosurf, Switzerland) to gain knowledge on the topography of the samples. The images were taken in tapping mode using a Tap190 cantilever (Budgetsensors, Bulgaria) with a nominal frequency of 190 kHz. Subsequently, the recorded images were corrected for artifacts and visualized using the Gwyddion software.<sup>46</sup>

## ■ RESULTS

**Morphology.** Caffeine was deposited by means of HWE on freshly cleaved muscovite mica (001). Various samples were prepared whereby the process conditions remained the same (substrate and wall temperature) except the molecular flux exposition time varying from 5 to 20 min. All samples reveal a very similar behavior with elongated needle-like structures being present at the mica surface (see Figure 1 and 2). At a deposition time of 20 min “broad” flat needles are present at the mica surface with extension of up to 100  $\mu\text{m}$  along the long needle axes. The width of the structures has a strong variation from 10  $\mu\text{m}$  down to approximately 1  $\mu\text{m}$ . A closer inspection reveals that individual needles consist of smaller elongated structures packed closely together (see Figure 6). The needle height of approximately 100 nm is similar over the entire sample. Beside the broad structures thin needles of significantly higher extension exist on the sample surface (visible as brighter whitish needles). The amount of those in the selected sample is relatively low.

Besides the needle morphology, the AFM image reveals that all needles at the surface align along defined directions with 60° or 120° inclination to each other. This is further supported by a 2D-FFT of this image which shows six streaks, every 60° on a 360° turn (see Figure 1b). This means three directions (or six if the 180° is taken into account separately) are present on the mica surface which facilitate the alignment of the caffeine

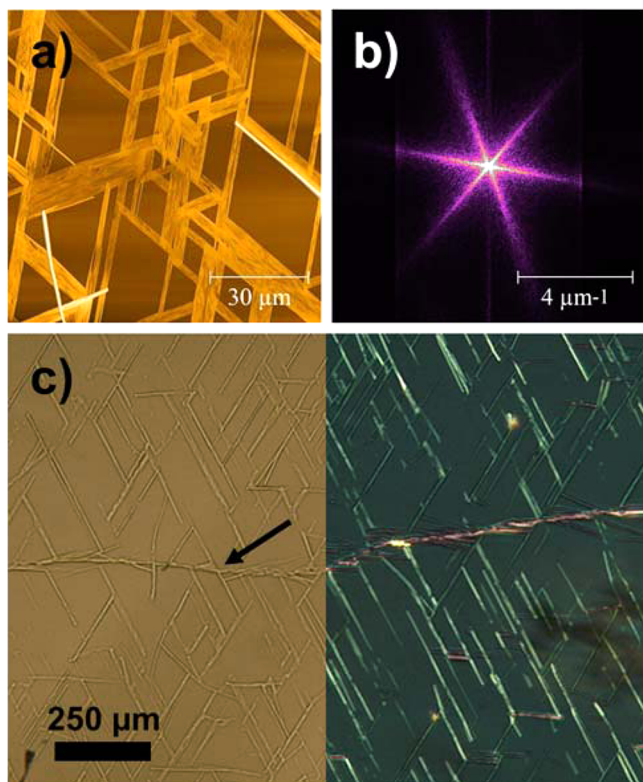


**Figure 1.** (a) Atomic force microscopy (AFM) height image of caffeine crystallites on a single mica domain. (b) Fourier transform of the AFM image. (c) Optical micrograph without (left) and with crossed-polarizers (right) showing caffeine on two separate mica domains (black arrow indicates cleavage step).

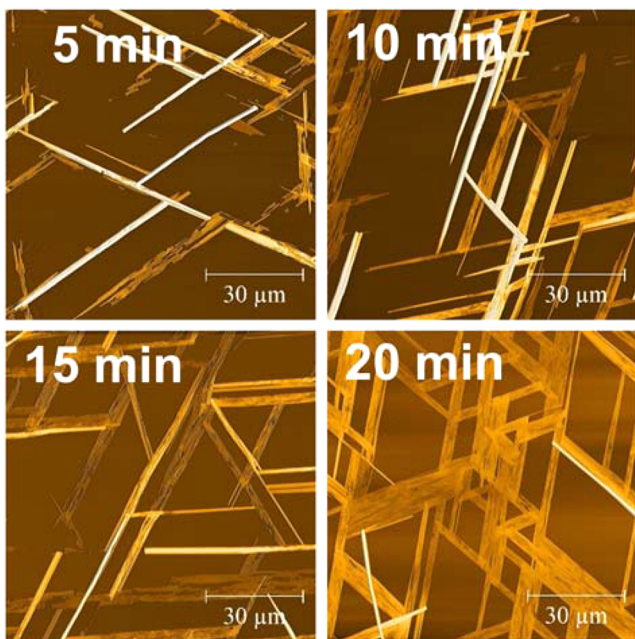


**Figure 2.** AFM images of caffeine crystallites on muscovite mica for various deposition times at 65 °C substrate temperature.

needles. As the mica surface may consist of two domains of 120° inclination<sup>29</sup> an additional optical micrograph (with and without crossed-polarizers) showing a cleavage step between such domains was taken (Figure 1c). Although crossed-

polarizers enhance the contrast of crystalline species, they also select needles depending on their orientation canceling certain directions in the image (compare Figure 1c, left and right side). However, the images reveal that in each domain all six directions are present which shows that the 60° symmetry is a result of caffeine aligning within one mica domain in all these directions. While most of the needle structures align consistently with defined angles, some needles with mismatched directions are noted (for an example see Figure 1a, lower left corner and Figure 1c, middle). Such needles occur due to nucleation at cleavage steps or other defects in the surface inducing growth in a direction mismatching the pattern.

On the change of deposition time the qualitative picture of caffeine on mica remains the same. At 5 min deposition time most of the caffeine assembles in the thin needle morphology with a height of typically 200 nm. Flat structures are present but compared to the 20 min sample these structures are strongly fragmented. Doubling the deposition time reveals that the flat structures coalesce and more interconnection points appear. At 15 min the ratio of thin and flat needles decreases, meaning that the amount of both become similar. At 20 min, the flat structures are most common which indicates that the initial needles broaden with increasing deposition time.

**Specular X-ray Diffraction Experiments.** To gain more insight into the crystallographic properties of caffeine on mica, X-ray based studies were performed. The specular X-ray diffraction pattern of the sample with 20 min deposition time is given in Figure 3. The region around 8.4 nm<sup>-1</sup> is shown as this

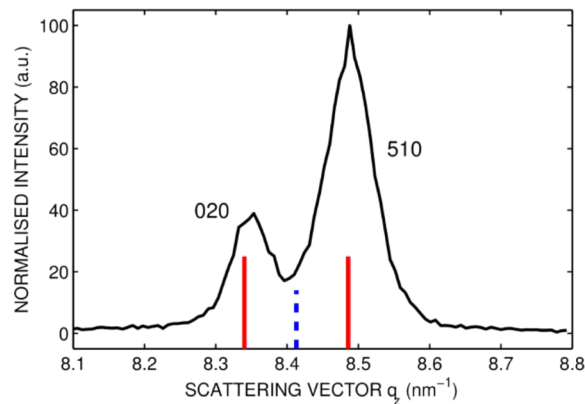


**Figure 3.** Specular X-ray diffraction scan of caffeine on mica. Calculated peak positions for the  $\beta$  (red, solid) and  $\alpha$  (blue, dashed) polymorph are indicated.

region corresponds to locations for which the most prominent net planes of caffeine are expected. The diffraction pattern of the sample shows two peaks located at  $q_z = 8.34$  and  $8.49$  nm<sup>-1</sup>, respectively while other peaks are not noted. The experimentally observed peaks correspond to a  $d$ -spacing of 0.75 and 0.74 nm, respectively. Since caffeine may exist in two polymorphic forms, the stable  $\beta$ -phase<sup>47</sup> (CSD code NIWFEE03) and the metastable  $\alpha$ -phase<sup>48</sup> (NIWFEE02), the peaks were compared to both crystal structure solutions, revealing an excellent match with the (020) and (510) net planes of caffeine in  $\beta$  conformation.

Because of the experimental geometry, a specular X-ray diffraction scan is only able to measure inter planar spacings ( $d$ -spacings) of net planes parallel to the substrate surface, thus the two peaks show that the sample contains various types of crystallites which differ in their contact planes; one has a (020)

and the other has a (510) contact plane (i.e., these net planes are parallel to the surface).

The preparation of caffeine samples at elevated temperature might facilitate the formation of a less stable high temperature polymorph.<sup>49,50</sup> A Bragg peak due to presence of less stable  $\alpha$ -form would be expected at  $q_z = 8.41 \text{ nm}^{-1}$ , between the  $\beta$ -phase peaks. However, this is not the case for samples prepared within this study (compare Figure 3), hence further explanations in this text are based on the  $\beta$ -polymorphic form and their behavior.

A comparison of the specular X-ray diffraction data for samples prepared with different deposition times reveals very similar diffraction patterns for all. The roughly constant intensity ratio of the 020 and 510 peaks indicates that the deposition time has no significant influence either on the selection of the contact plane nor the polymorph (measurements are provided in the Supporting Information). Despite the difference in the amount of thin and flat needles for the various samples, it cannot be concluded that each of the species has a different contact plane since the relative peak heights seems unaffected by this fact. Thus, it seems to be equally likely that both planes, (020) and (510), have a certain probability to contact the surface.

**X-ray Pole Figures Experiments.** The presence of the small number of Bragg peaks in the specular X-ray diffraction scans typically means that a preferred crystal alignment is present. This is further supported by microscopy investigations which even suggest that a biaxially alignment could have taken place during crystal growth. For the crystallographic investigation of such samples the X-ray pole figure technique is best suited. Within such a pole figure measurement the scattering vector  $\mathbf{q}$  is fixed (thus a specific  $d$ -spacing and its corresponding net planes is selected) while the sample is rotated ( $\varphi$ ) and/or tilted ( $\psi$ ). High intensity (poles) occurs in this experiment for crystallites aligning in a proper direction fulfilling the Laue condition and consequently the intensity distribution allows for the integral crystallographic arrangement of crystals on the sample to be identified.

Pole figure measurements for two scattering vectors performed at the thickest sample (thus giving the most diffracted intensity) are shown in Figure 4. In Figure 4a the pole figure measured at  $|q| = 8.4 \text{ nm}^{-1}$ , thus selecting net planes with inter planar spacings of approximately 0.75 nm, reveals seven poles, which considering the low resolution at this  $|q|$ -value must be a result of either the 020 or 510 Bragg reflections fulfilling the Laue condition. In the center of this pole figure ( $\psi = 0^\circ$ ) the high intensity results from the net planes which are parallel to the substrate surface. According to the specular X-ray scans it needs to be the (020) or (510) plane. Away from the center six other poles are present. All these poles are located at a common inclination ( $\psi = 60^\circ$ ) to the surface normal. In the azimuthal direction poles are located at  $\varphi = 30^\circ, 90^\circ, 150^\circ, 210^\circ, 270^\circ$ , and  $330^\circ$ , meaning that each pole is rotated by  $60^\circ$  with respect to its adjacent. This is in excellent agreement with the Fourier transform (see Figure 1b) of the AFM image which also showed streaks with an azimuthal rotation of  $60^\circ$ . This suggests that the pole figure is a result of six needle growth directions.

To gain further information about the sample an additional pole figure at  $|q| = 19.0 \text{ nm}^{-1}$  was recorded (Figure 4b). At this scattering angle inter planar distances of about 0.33 nm will produce poles on the fulfillment of the Laue condition. A comparison with the crystal structure shows that net planes

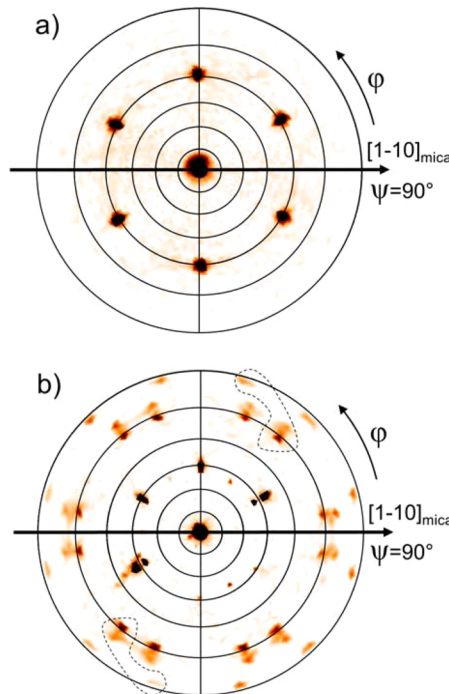


**Figure 4.** X-ray pole figures of caffeine on mica measured at a scattering vector  $|q| = 8.4$  (a) and  $19.0 \text{ nm}^{-1}$  (b). Summarized poles within the dashed regions appear regularly due to crystallites of different azimuthal orientation. Solid black line indicates the mica mirror symmetry direction.

with  $hkl = \{60\bar{2}\}, \{11\bar{2}\}$  (curly brackets indicate all permitted permutations of  $hkl$ ) are measured. In the middle of the pole figure ( $\psi = 0^\circ$ ) the peak corresponding to the mica (006) net plane is present. At inclination angles of  $\psi = 45^\circ$  six poles are noted which are also a result of the substrate. The various peaks at  $\psi = 75^\circ, 80^\circ$ , and  $88^\circ$  correspond to caffeine and can be explained by one unique repetitive pattern (indicated by dashed region). This pattern is repeated every  $60^\circ$  in azimuthal direction, which is again in well agreement with the observed needle directions which are also separated by  $60^\circ$ .

## ■ DISCUSSION

The crystallization of caffeine in solution results in needle type morphology in the  $\beta$ -phase. On heterogeneous crystallization from solution two morphologies are typically evident, with long needles and the extended hexagonal structures.<sup>38</sup> The investigation of caffeine on mica surface prepared via HWE reveals similarly to bulk solutions solely needle type structures of caffeine in  $\beta$ -phase. Indication of another polymorph, especially the metastable  $\alpha$ -phase was not noted, hence crystallization on mica is similar to the bulk.

Muscovite mica has a rather complex crystalline structure.<sup>17,26</sup> However, it provides a highly ordered surface structure because of weakly bond aluminum-silica sheets. By cleaving along these sheets, relatively large areas of atomically flat and clean (001) surfaces can be obtained. Adjacent mica sheets are very much alike, but one ( $\alpha$ -mica) is rotated by  $120^\circ$  with respect to the other sheet ( $\beta$ -mica). Typically, a sample of cleaved mica surface consists of several individual domains with each containing just  $\alpha$  or  $\beta$  mica (see Figure 1c). The surface unit cell of the  $\alpha$  domain exhibits a mirror symmetry along the mica [110] direction and a slight corrugation because of slightly lower oxygen along the same direction (for the  $\beta$ -sheet

everything is equivalent, but rotated by  $120^\circ$  with respect to the  $\alpha$ -sheet).<sup>29</sup> Strictly speaking, a mica surface has only a mirror symmetry but allowing for some deviations one could easily identify a pseudo-3-fold symmetry arrangement of the oxygen atoms at the surface.<sup>26</sup> From this simple consideration it follows that for directed growth along the oxygen grooves only one crystal direction should be present in a domain. For growth that is affected by the mirror symmetry two directions should be noted while 3-fold symmetry means that most likely the nearly hexagonal oxygen arrangement in the surface is responsible for the molecular alignment. The AFM and optical measurements clearly show that six needle directions are present. Furthermore, these six directions are present in their close vicinity ( $\sim$ couple of micrometers), meaning these six growth directions are present in one single mica domain. This is further supported by optical microscopy which clearly allows to separate the domains with each containing six caffeine directions. Thus, the needle growth is a result of caffeine crystals aligning on the account of the slightly disturbed 3-fold “oxygen symmetry” in the mica surface. Such a behavior might seem obvious, however previous studies of rod-like conjugated molecules such as para-sexiphenyl (p6P) on muscovite mica showed remarkably different results. Although showing a similar needle-like morphology the azimuthal alignment was not determined by the 3-fold symmetry since only growth along one direction was observed and thus the surface corrugations because of lowered oxygen atoms in the surface are assumed to cause the alignment.<sup>51</sup> Another example for rod-like molecules on mica is ternaphthalene (NNN), also showing clearly directed growth of needle-like crystallites but with two directions being present on the surface. Hence it was concluded that the mirror-symmetry of the mica surface is determining for the growth directions.<sup>52</sup> Such a comparison with rod-like molecules illustrates peculiarly well that a wide range of molecules with various geometries and chemical properties are necessary to understand the diverse mechanisms of directed growth on solid surfaces.

To obtain information on the crystallographic orientation of the caffeine needles with respect to the mica surface, each pole in Figure 4 is indexed, that is, each pole gets assigned a corresponding net plane ( $hkl$ ). The poles observed in Figure 4a are limited to net planes of the  $\{510\}$  and  $\{020\}$  family because of the fixed scattering vector of  $|q| = 8.4 \text{ nm}^{-1}$ . The center peak ( $\psi = 0$ ) in the pole figure, as already established by specular diffraction experiments, corresponds to the  $(510)$  and/or  $(020)$  net planes. Since crystallites with those contact planes have very similar  $d$ -spacings, 0.753 and 0.740 nm, respectively, it was not possible to separate both contribution due to the limited resolution of the setup in use. However, for the sake of simplicity it is assumed that only needles with a  $(510)$  contact plane are present. In the Supporting Information an alternative indexation using a  $(020)$  contact plane is provided.

In Figure 5b the inclinations ( $\psi$  in the pole figure) of the  $(\bar{5}10)$  and  $(020)$  net planes with respect to the  $(510)$  contact plane is illustrated. As clearly seen, the inclination angles of the  $(\bar{5}10)$  and  $(020)$  with respect to the contact plane are in the case of caffeine extremely similar ( $58.9^\circ$  and  $60.6^\circ$ , respectively) and explains the common inclination of the poles of approximately  $60^\circ$ . While the inclinations are defined by the net planes within a crystallite, the azimuthal angle  $\varphi$  depends on the direction of the crystallite on the surface. Therefore, to obtain a proper description of the pole figure, it is necessary to find the correct azimuthal orientation by rotating the crystallite

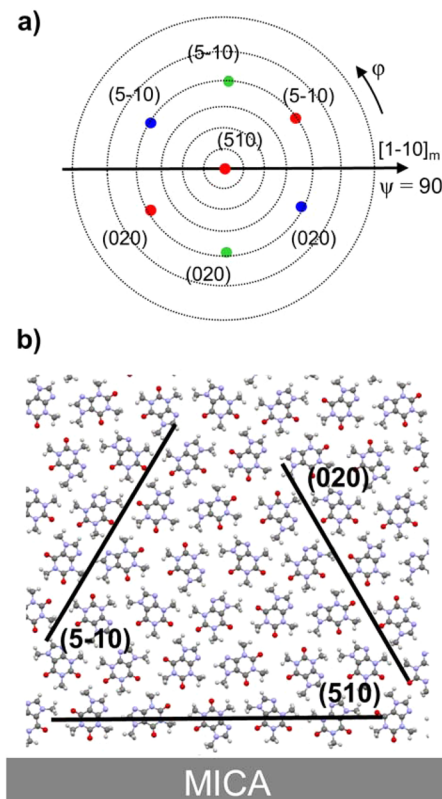


**Figure 5.** (a) Simulated pole distribution for poles observed at  $|q| = 8.4 \text{ nm}^{-1}$  using three crystals (red, green, blue) with  $(510)$  contact planes. (b) View of a caffeine crystallite along the  $c$ -axis (long needle axis) with  $(510)$  contact plane. Black lines illustrate the projection of the  $(510)$ ,  $(\bar{5}10)$ , and  $(020)$  net planes.

around its contact plane normal until the calculated poles match the spots of enhanced intensities in the pole figure.

However, using just one crystallite of a specific orientation gives only two poles, as indicated by different colors in Figure 5a. To get a complete description of the pole figure, at least two additional crystallites with different azimuthal alignment need to be introduced (blue, green). Each crystallite is rotated azimuthally by  $60^\circ$  with respect to each other. These crystallites with distinct directions are in excellent agreement with six different needle directions as seen in optical and AFM micrographs (compare Figure 1). As mentioned earlier, a  $(020)$  contact plane would yield a similar result. This becomes quite obvious, if one considers a clockwise rotation of the crystal by  $60^\circ$  along the needle axis. The  $(020)$  plane would become the contact plane with the mica surface (parallel to the surface) and consequently the  $(510)$  is then  $180^\circ$  rotated in  $\varphi$  with respect of the  $(5-10)$  plane and both are found at a common inclination of  $\sim 60^\circ$ .

The pole figure taken at  $|q| = 8.4 \text{ nm}^{-1}$  can be understood in the crystals having a  $(020)$  or  $(510)$  contact plane with the surface. However, the unit cell equivalent contact planes should exist with the  $hkl$  of, for instance  $(0-20)$  and  $(-\bar{5}10)$ . While this cannot be proved at the measurement taken at  $|q| = 8.4 \text{ nm}^{-1}$  the pole figure taken at  $|q| = 19.0 \text{ nm}^{-1}$  allows for a clarification. At various  $\psi$  values larger than  $70^\circ$  12 poles at defined  $\varphi$  values are present which can be paired to six groups. Each group is rotated by  $60^\circ$  of another. Within a group a splitting exists, for instance  $18^\circ$  at  $\psi = 75^\circ$ . This group splitting is a result of some caffeine having a  $(510)$  and some other

having  $(\bar{5}\bar{1}0)$  contact plane. The monoclinic angle  $\beta = 99^\circ$  of the caffeine unit cell accounts for such a splitting on inverting the crystal, thus proving that more than two contact planes are required to understand the caffeine growth on mica. For sake of completeness, a more detailed description of the indexation is provided in the [Supporting Information](#).

Having the pole figure indexed, provides the opportunity to see the crystallographic relation of the caffeine unit cell with the mica surface. In the caffeine unit cell the disk-like molecules stack onto each other along the  $a$  and  $b$  axis in an edge-on conformation while a parallel stacking similar to a  $\pi-\pi$  stacking is formed along the  $c$ -axis. The latter, so the  $c$ -axis, is also identical to the morphological needle axis of caffeine. From the pole figure it follows that the  $c$ -axis of caffeine points toward  $\varphi = 0^\circ, 60^\circ, 120^\circ$ , as well as  $180^\circ, 240^\circ$ , and  $300^\circ$ , giving basically six crystallographic growth directions. However, only three morphological directions are observable within the AFM; needles which are inclined by  $180^\circ$  cannot be distinguished. Furthermore, for all azimuthal directions the  $c$ -axis points toward  $\psi = 90^\circ$ , meaning the  $c$ -axis is parallel to the surface. A comparison of these directions with the main directions of a mica surface, that is,  $[1\bar{1}0]$ ,  $[100]$ ,  $[110]$ , shows that the long needle axis ( $c$ -axis) coincides with this main directions supporting the fact that the pseudo-3-fold symmetry of the mica surface dictates the caffeine crystal growth (see Figure 6).

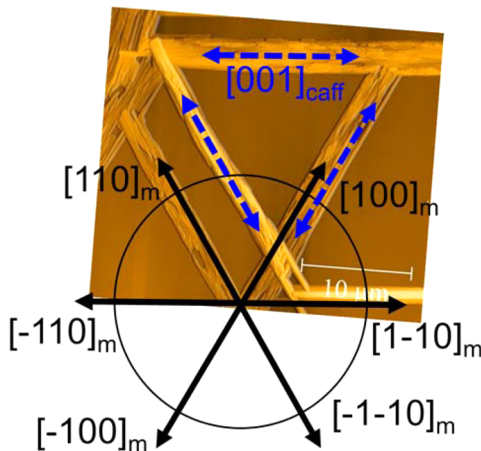


**Figure 6.** Atomic force microscopy image showing the relation between the azimuthal alignment of caffeine crystallites (blue arrows indicate  $c$ -axis) and the mica real space directions (black arrows).

This is in agreement with the previous assumption derived from the morphological investigation, but now with the interpretation of the pole figure also the crystallographic information is accessible.

The  $a$ -axis of caffeine is also in-plane as long as the contact plane is a  $(020)$ . However, a common azimuthal direction with the underlying mica substrate is not observed. For the  $(510)$  contact plane the  $a$  and  $b$  axis do not coincide with any mica main direction. Regardless of the contact plane, the  $c$ -axis remains unaffected, meaning that the azimuth of the needle axis is well aligned while there is some freedom for the contact plane to be chosen. On a closer inspection of the molecular arrangement within the unit cell shows that  $(020)$  and a  $(510)$  plane have a very much alike caffeine assembling with the surface; “edge-on” with slightly rotated adjacent molecules. This also suggests that the energy for both situations is very

similar, meaning no preferential growth of either  $(020)$  or  $(510)$  crystallites takes place.

The heterogeneous nucleation and crystallization at a solid surface is a complex process. Typically an individual molecule adsorbs on the surface most likely such that the caffeine molecule is lying flat. From simple energetic considerations a single flat-lying molecule should be energetically favored as the van der Waals interactions allow to minimize the energy more effectively. As time progresses more molecules accommodate in the vicinity. Anisotropic molecular diffusion along the surface allows for nucleus formation and further crystal growth. In the case of caffeine, the crystals have an edge-on conformation of upright standing molecules, thus limiting their interaction with surface to the terminal methyl groups or oxygen atoms. It seems that the increased energetic cost of several upright standing molecules is outweighed by an overall smaller energy of the well aligned crystals.<sup>53</sup> Furthermore, the investigations show that the molecules align perpendicular to the mica main directions. At this stage it is not clear if the nucleation and crystal growth takes place already in that very confinement or if a rearrangement of the nucleus or crystal takes place. However, there are many theoretical consideration trying to explain such a situation like lattice match<sup>54,55</sup> or density functional theory calculations. Typically, many preassumptions have to be taken into account for such a theoretical approach which makes a possible explanation of caffeine on mica via such tools challenging.

Surprisingly, the growth of caffeine on mica via HWE reveals a distinct crystal alignment as obtained from solution cast films. First, HWE facilitates predominantly the growth of crystallites with  $\{510\}$  and  $\{020\}$  contact planes, while solution processing shows additional  $\{110\}$ ,  $\{520\}$ , and  $\{530\}$  contact planes. This means the solution cast crystallites have some rotational freedom along the  $c$ -axis, that is, allows for rotation of those. Other than the  $(510)$  and  $(020)$  contact planes which provide “flat crystal cuts” (compare Figure 5) these additional contact planes might develop facets. The second surprising difference is the alignment of the caffeine crystal axes with respect to mica. In the case of HWE the  $c$ -axis, which defines the long needles axis, is aligned along the mica main axes regardless of the contact plane. The solution processing lead to an alignment of the  $a$ -axis, thus the  $c$ -axis does not coincide with any mica main direction. On one hand this means that caffeine deposited via HWE only shows six growth direction while solution cast have another six which are inclined by  $18^\circ$  to the others. On the other hand this also means the disk-like caffeine molecules stand perpendicular to the mica main axes for the HWE sample whereas the molecules stand parallel in the case the solution cast. The reasons for the appearance of this differences could be manifold. The preparation route seems to play an important role, since the different alignments were observed exclusively on either type of sample. The main difference between these preparation techniques might be the solvent during the adsorption, nucleation and subsequent crystal growth. It might cause other sticking/adsorption sites at the mica surface to be selected. However, also other factors might account for this deviation such as the elevated substrate temperature during HWE, which changes the diffusion/sticking behavior of molecules on surfaces. Furthermore, the time scale of crystal growth differs drastically. In the case of HWE the caffeine deposition takes up to 20 min and is carried out very close to thermodynamic equilibrium. In contrast, deposition from solution, using especially a fast evaporating solvent such as

tetrahydrofuran, is approximately one to 2 orders of magnitude faster. It is well established that kinetics have a decisive impact on crystal growth and might even prevail free energy minimization.

## CONCLUSION

Depositing anhydrous caffeine on muscovite mica using hot wall epitaxy (HWE) facilitates the growth of the typical needle-like caffeine crystals along six azimuthal directions with respect to the surface. The needles show an inclination of  $120^\circ$  with respect to each other which is attributed to the slightly disturbed 3-fold symmetry of the underlying mica surface. While this is obvious from simple microscopy images, pole figure measurements reveal a more detailed picture. The long needle axis, defined by the crystallographic *c*-axis, aligns along the [110], [100], [110] real space directions of mica. This means, the disk-like molecules are oriented upright standing (edge-on) with respect to the surface and perpendicular to the aforementioned mica directions. Such directed crystal growth along preferred directions means that the interaction of the regular mica surface and the periodic structure provided by the molecules within the caffeine crystallites is most likely energetically favored along these directions.

The aspect of *c*-axis alignment is of particular interest when compared to a previous study on solution cast caffeine on mica since an alignment of the *a*-axis was achieved by this preparation route. The difference in alignment has an immediate impact on the observed needle directions. For HWE processed needles the long needle axis always points in the same directions as the aligned *c*-axis independent of the crystal orientation (e.g., flipping a crystal), while an *a*-axis alignment gives additional needles directions since the *a* and *c*-axis are inclined by approximately  $9^\circ$  due to the monoclinic unit cell of caffeine. Whereas both methods, HWE and solution casting, yield similar needle-like morphologies, the actual molecular interaction and arrangement with respect to the surface is surprisingly different, showing that further studies regarding the process parameters such as solvent, surface and temperature are essential to gain further understanding of the complex behavior of asymmetric molecules on solid surfaces.

## ASSOCIATED CONTENT

### Supporting Information

The Supporting Information is available free of charge on the ACS Publications website at DOI: [10.1021/acs.cgd.5b00833](https://doi.org/10.1021/acs.cgd.5b00833).

Specular X-ray diffraction data of caffeine on mica for various deposition times, indexation, and detailed explanations of pole figures recorded at  $|q| = 8.4 \text{ nm}^{-1}$  and  $|q| = 19.0 \text{ nm}^{-1}$ . ([PDF](#))

## AUTHOR INFORMATION

### Corresponding Authors

\*E-mail: [christian.roethel@uni-graz.at](mailto:christian.roethel@uni-graz.at).

\*E-mail: [oliver.werzer@uni-graz.at](mailto:oliver.werzer@uni-graz.at).

### Notes

The authors declare no competing financial interest.

## ACKNOWLEDGMENTS

The work was funded by the Austrian Science Fund (FWF): P25541-N19 and P25154-N20. The authors gratefully acknowledge support from NAWI Graz.

## REFERENCES

- (1) Dimitrakopoulos, C. D.; Malenfant, P. R. L. *Adv. Mater.* **2002**, *14*, 99–117.
- (2) Peumans, P.; Uchida, S.; Forrest, S. R. *Nature* **2003**, *425*, 158–162.
- (3) Kim, H.; Gilmore, C. M.; Piñé, A.; Horwitz, J. S.; Matoussi, H.; Murata, H.; Kafafi, Z. H.; Chrisey, D. B. *J. Appl. Phys.* **1999**, *86*, 6451–6461.
- (4) Lassnig, R.; Striedinger, B.; Hollerer, M.; Fian, A.; Stadlober, B.; Winkler, A. *J. Appl. Phys.* **2014**, *116*, 114508.
- (5) Ehmann, H. M. A.; Baumgartner, R.; Kunert, B.; Zimmer, A.; Roblegg, E.; Werzer, O. *J. Phys. Chem. C* **2014**, *118*, 12855–12861.
- (6) Virkar, A. A.; Mannsfeld, S.; Bao, Z.; Stingelin, N. *Adv. Mater.* **2010**, *22*, 3857–3875.
- (7) Simbrunner, C.; Quochi, F.; Hernandez-Sosa, G.; Oehzelt, M.; Resel, R.; Hesser, G.; Arndt, M.; Saba, M.; Mura, A.; Bongiovanni, G.; Sitter, H. *ACS Nano* **2010**, *4*, 6244–6250.
- (8) Simbrunner, C.; Hernandez-Sosa, G.; Quochi, F.; Schwabegger, G.; Botta, C.; Oehzelt, M.; Salzmann, I.; Djuric, T.; Neuhold, A.; Resel, R.; Saba, M.; Mura, A.; Bongiovanni, G.; Vollmer, A.; Koch, N.; Sitter, H. *ACS Nano* **2012**, *6*, 4629–4638.
- (9) Musumeci, C.; Salzmann, I.; Bonacchi, S.; Röthel, C.; Duham, S.; Koch, N.; Samori, P. *Adv. Funct. Mater.* **2015**, *25*, 2501–2510.
- (10) Tsoi, W. C.; Spencer, S. J.; Yang, L.; Ballantyne, A. M.; Nicholson, P. G.; Turnbull, A.; Shard, A. G.; Murphy, C. E.; Bradley, D. D. C.; Nelson, J.; Kim, J.-S. *Macromolecules* **2011**, *44*, 2944–2952.
- (11) Hilfiker, R. *Polymorphism: In the Pharmaceutical Industry*; Wiley-VCH: Weinheim, Germany, 2006.
- (12) Rodríguez-Spong, B.; Price, C. P.; Jayasankar, A.; Matzger, A. J.; Rodríguez-Hornedo, N. *Adv. Drug Delivery Rev.* **2004**, *56*, 241–274.
- (13) Singhal, D.; Curatolo, W. *Adv. Drug Delivery Rev.* **2004**, *56*, 335–347.
- (14) Baptiste, L.; van Landschoot, N.; Gleijm, G.; Priede, J.; Schade van Westrum, J.; Velthuis, H.; Kim, T.-Y. *Surf. Coat. Technol.* **2007**, *202*, 1189–1193.
- (15) *Springer Handbook of Nanotechnology*; Bhushan, B., Ed.; Springer: Berlin, 2010.
- (16) Jones, A. O.; Geerts, Y. H.; Karpinska, J.; Kennedy, A. R.; Resel, R.; Röthel, C.; Ružić, C.; Werzer, O.; Sferrazza, M. *ACS Appl. Mater. Interfaces* **2015**, *7*, 1868–1873.
- (17) Simbrunner, C.; Hernandez-Sosa, G.; Oehzelt, M.; Djuric, T.; Salzmann, I.; Brinkmann, M.; Schwabegger, G.; Watzinger, I.; Sitter, H.; Resel, R. *Phys. Rev. B: Condens. Matter Mater. Phys.* **2011**, *83*, 115443.
- (18) Ehmann, H. M. A.; Werzer, O. *Cryst. Growth Des.* **2014**, *14*, 3680–3684.
- (19) Schieber, S.; Huth, M.; Dobrinevski, A.; Nickel, B. *J. Am. Chem. Soc.* **2007**, *129*, 10316–10317.
- (20) Kim, J. S.; Granström, M.; Friend, R. H.; Johansson, N.; Salaneck, W. R.; Daik, R.; Feast, W. J.; Cacialli, F. *J. Appl. Phys.* **1998**, *84*, 6859–6870.
- (21) Werzer, O.; Matoy, K.; Smilgies, D.-M.; Rothmann, M. M.; Strohriegel, P.; Resel, R. *J. Appl. Polym. Sci.* **2008**, *107*, 1817–1821.
- (22) Onclin, S.; Ravoo, B. J.; Reinhoudt, D. N. *Angew. Chem., Int. Ed.* **2005**, *44*, 6282–6304.
- (23) Birkholz, M.; Fewster, P. F.; Genzel, C. *Thin Film Analysis by X-ray Scattering*; Wiley-VCH: Weinheim, Germany, 2006.
- (24) Kittel, C. *Introduction to Solid State Physics*; John Wiley and Sons, Ltd.: Hoboken, NJ, 2004.
- (25) Surnev, S.; Kresse, G.; Sock, M.; Ramsey, M. G.; Netzer, F. P. *Surf. Sci.* **2001**, *495*, 91–106.
- (26) Kuwahara, Y. *Phys. Chem. Miner.* **2001**, *28*, 1–8.
- (27) Chadi, D. J. *Phys. Rev. Lett.* **1979**, *43*, 43–47.
- (28) Giling, L. J.; Van Enckevort, W. J. P. *Surf. Sci.* **1985**, *161*, 567–583.
- (29) Simbrunner, C.; Nabok, D.; Hernandez-Sosa, G.; Oehzelt, M.; Djuric, T.; Resel, R.; Romaner, L.; Puschning, P.; Ambrosch-Draxl, C.; Salzmann, I.; Schwabegger, G.; Watzinger, I.; Sitter, H. *J. Am. Chem. Soc.* **2011**, *133*, 3056–3062.

- (30) Salzmann, I.; Duhm, S.; Heimel, G.; Rabe, J. P.; Koch, N.; Oehzelt, M.; Sakamoto, Y.; Suzuki, T. *Langmuir* **2008**, *24*, 7294–7298.
- (31) Koch, N.; Vollmer, A.; Salzmann, I.; Nickel, B.; Weiss, H.; Rabe, J. P. *Phys. Rev. Lett.* **2006**, *96*, 156803.
- (32) Radziwon, M.; Madsen, M.; Balzer, F.; Resel, R.; Rubahn, H.-G. *Thin Solid Films* **2014**, *558*, 165–169.
- (33) Gibson, M. *Pharmaceutical Preformulation and Formulation: A Practical Guide from Candidate Drug Selection to Commercial Dosage Form*; Taylor & Francis: New York, 2001.
- (34) Trask, A. V.; Jones, W. In *Organic Solid State Reactions*; Toda, F., Ed.; Topics in Current Chemistry; Springer: Berlin, 2005; pp 41–70.
- (35) Cronstein, B. N. *J. Hepatol.* **2010**, *53*, 207–208.
- (36) Sawynok, J.; Yaksh, T. L. *Pharmacol. Rev.* **1993**, *45*, 43–85.
- (37) Descamps, M.; Correia, N. T.; Derolle, P.; Danede, F.; Capet, F. *J. Phys. Chem. B* **2005**, *109*, 16092–16098.
- (38) Sarfraz, A.; Simo, A.; Fenger, R.; Christen, W.; Rademann, K.; Panne, U.; Emmerling, F. *Cryst. Growth Des.* **2012**, *12*, 583–588.
- (39) Leiterer, J.; Emmerling, F.; Panne, U.; Christen, W.; Rademann, K. *Langmuir* **2008**, *24*, 7970–7978.
- (40) Werzer, O.; Kunert, B.; Roblegg, E.; Zimmer, A.; Oehzelt, M.; Resel, R. *Cryst. Growth Des.* **2013**, *13*, 1322–1328.
- (41) Mattox, D. M. *Handbook of Physical Vapor Deposition (PVD) Processing*; William Andrew: Oxford, U.K., 2010.
- (42) Lopez-Otero, A. *Thin Solid Films* **1978**, *49*, 3–57.
- (43) Sitter, H.; Andreev, A.; Matt, G.; Sariciftci, N. S. *Mol. Cryst. Liq. Cryst.* **2002**, *385*, 51–60.
- (44) Schulz, L. G. *J. Appl. Phys.* **1949**, *20*, 1030–1033.
- (45) Salzmann, I.; Resel, R. *J. Appl. Crystallogr.* **2004**, *37*, 1029–1033.
- (46) Nečas, D.; Klapetek, P. *Cent. Eur. J. Phys.* **2011**, *10*, 181–188.
- (47) Lehmann, C. W.; Stowasser, F. *Chem.—Eur. J.* **2007**, *13*, 2908–2911.
- (48) Enright, G. D.; Terskikh, V. V.; Brouwer, D. H.; Ripmeester, J. A. *Cryst. Growth Des.* **2007**, *7*, 1406–1410.
- (49) Hédoux, A.; Decroix, A.-A.; Guinet, Y.; Paccou, L.; Derolle, P.; Descamps, M. *J. Phys. Chem. B* **2011**, *115*, 5746–5753.
- (50) Hédoux, A.; Guinet, Y.; Paccou, L.; Danède, F.; Derolle, P. *J. Pharm. Sci.* **2013**, *102*, 162–170.
- (51) Resel, R.; Haber, T.; Lengyel, O.; Sitter, H.; Balzer, F.; Rubahn, H.-G. *Surf. Interface Anal.* **2009**, *41*, 764–770.
- (52) Simbrunner, C.; Schwabegger, G.; Resel, R.; Dingemans, T.; Sitter, H. *Cryst. Growth Des.* **2014**, *14*, 442–449.
- (53) Potocar, T.; Lorbek, S.; Nabok, D.; Shen, Q.; Tumbek, L.; Hlawacek, G.; Puschnig, P.; Ambrosch-Draxl, C.; Teichert, C.; Winkler, A. *Phys. Rev. B: Condens. Matter Mater. Phys.* **2011**, *83*, 075423.
- (54) Hoshino, A.; Isoda, S.; Kurata, H.; Kobayashi, T. *J. Appl. Phys.* **1994**, *76*, 4113–4120.
- (55) Smilgies, D.-M.; Kintzel, E. *J. Phys. Rev. B: Condens. Matter Mater. Phys.* **2009**, *79*, 235413.